IET Electric Power Applications

*Research Article*

IET Journals
The Institution of Engineering and Technology

# Self-commissioning of flux linkage curves of synchronous reluctance machines in quasi-standstill condition

ISSN 1751-8660
Received on 6th March 2015
Revised on 28th May 2015
Accepted on 25th June 2015
doi: 10.1049/iet-epa.2015.0070
www.ietdl.org

*Luca Peretti* ✉, *Paul Sandulescu*, *Giovanni Zanuso*

*Department of Electrical Systems, ABB Corporate Research, Forskargränd 7, 72178 Västerås, Sweden*
✉ *E-mail: luca.peretti@se.abb.com*

**Abstract:** This study presents a self-commissioning procedure for the estimation of the flux linkage curves of synchronous reluctance machines. The procedure exploits a quasi-standstill condition obtained by imposing fast torque oscillations. The flux linkage is calculated by means of a pure integration of the voltages and currents. With respect to the existing procedures, the proposed one tackles the problem of the limited knowledge of the core losses in the electrical machine, which is shown to induce erroneous estimation results for the case under investigation. A theoretical analysis supported by extensive laboratory measurements is shown, proving the effectiveness of the proposed approach.

## 1 Introduction

The self-commissioning of electrical machine parameters is still a lively research topic, in particular when dealing with machines with strong magnetic non-linearities as interior permanent magnet synchronous machines (IPM-SMs) and synchronous reluctance machines (SynRMs). The estimation of the magnetic model, which is required for the control strategy, is obtained automatically by means of an inverter connected to a machine. The human intervention is limited to the machine nameplate data entries in the control software. While involving interesting mathematical and operational aspects, self-commissioning procedures have a clear impact in industrial drives and related applications, where the quest for ease of use and precise parameter estimation despite manufacturing differences is a driving force within the industrial R&D.

The electrical machine commissioning problem, with particular attention to the self-commissioning problem at standstill, has been investigated in previous works. Standard measurements to evaluate the magnetic characteristics of synchronous machines are known, and have been recently recalled in detailed publications such as Armando *et al.* [1], Pellegrino *et al.* [2], Cintron-Rivera *et al.* [3], with a follow-up on the sensitivity analysis of the latter algorithm as described in [4]. These solutions are suitable for the generation of detailed curves of the magnetic model, and thus can be used as a reference for comparing any other estimation procedure. On the other side, these solutions either require a speed-regulated load machine, or a freely rotating rotor disconnected from any sensitive load. Thus, they require a higher level of human intervention with respect to automatic self-commissioning methods.

A series of works on machine commissioning has been performed in [5–11]. The common point of these procedures is the exploitation of a pulsating torque generated by different combinations of currents in the rotating $dq$ reference frame of a synchronous machine. These combinations are obtained by setting one current at a constant level (eg. the $d$-axis current) while varying the other current (eg. the $q$-axis current) in an alternating way, using square-wave voltages with zero mean value. The flux linkage is obtained as the integral of the voltage minus the stator resistance voltage drop. Interestingly, these tests are able to display non-linear hysteresis effects in the magnetic materials. Different solutions for obtaining an estimation in the presence of hysteresis are proposed: by drawing different hysteresis loops at different current levels and connecting their vertices, or by averaging the lower curve and the upper curve of the largest hysteresis cycle. While the concept is valid, and a variant of the method I described in [6] is used in this work, sometimes the machines seem to require a locked rotor configuration in order to avoid rotor movements. Moreover, the measurements are not compared with standard methods as in [1–3].

It is accepted that commissioning estimation techniques, especially the standstill or quasi-standstill ones, are affected by the presence of core losses. The modelling of the latter has been imported from the established techniques developed for induction machines [12, 13] and later for the synchronous machines [14]. A solution for including core losses in automatic parameter estimation techniques is described in [15], further investigated in [16]. Recently, Lar and Radulescu [17] have also contributed to the field. All these techniques, however, are not performed at standstill and require a speed measurement.

The interest in taking into account undesired effects while estimating magnetic models is also a target of self-commissioning methods for position-sensorless estimation techniques, especially for those based on high-frequency signal injection. Many examples are reported in the literature [18–22]. While concluding that magnetic models are frequency dependent, the reported solutions do not discuss the core losses phenomena at lower frequencies.

A recent work that proposes a standstill method for the identification of the direct-axis inductance is reported in [23]. Core losses are considered with an equivalent resistance and the estimation time is reduced by applying multi-frequency injection signals. No quadrature inductance is estimated. Another self-commissioning solution was presented in [24]. The target was to identify a load-dependent anisotropy displacement without a position sensor. Since a pulse current in the quadrature axis is applied, the method induces a minimal rotor movement although it does not consider the estimation of the complete flux linkage map, nor takes into account possible estimation deviations due to the presence of core losses.

In recent years, a series of publications showing the estimation of differential inductances by using square-wave reference currents (thus going towards the solution of [7]) have appeared [25–28]. While interesting for the relative ease of implementation, these quasi-standstill solutions do not consider the effect of core losses. Kuehl and Kennel [29] make a comparison between a method similar to [3] and a high-frequency injection method for differential inductance estimation, and concludes that the differential inductances obtained by high-frequency measurements are always smaller, for frequencies as low as 250 Hz. Among the possible causes, core losses are mentioned.

This work contributes on the topic of self-commissioning methods for the estimation of the flux linkage curves of a SynRM, by means of an oscillating torque generation and a quasi-standstill rotor condition. The motivation of the work is to provide complete maps for a correct maximum-torque-per-ampere operation of the machine, and precise parameter values for model-based speed sensorless control algorithms. The proposed procedure tackles the core losses issue by properly handling the magnetic hysteresis data to trace the flux linkage curves. The method employs current regulators which are tuned only once at the beginning of the procedure, and does not require a locked rotor condition.

The paper is divided as follows. Section 2 summarises the basic SynRM dynamic equations. Section 3 discusses how the flux linkages can be estimated (Section 3.1), focusing on the differential-inductance-based methods in Section 3.2 and on the proposed method in Section 3.3. The experimental setup is described in Section 4.1, while the reference flux linkage curves are measured and presented in Section 4.2. A preliminary experimental analysis showing the effect of core losses in the differential-inductance-based estimation methods is shown in Section 4.3. The estimation results of the proposed method are shown in Section 4.4. Some final remarks are given in Section 5.

## 2 Theoretical background

The $dq$ rotating reference frame of the SynRM under analysis is defined first. In this work, the $d$-axis is aligned to the axis with the minimum magnetic reluctance (larger flux linkage), while the $q$-axis is aligned to the axis of maximum magnetic reluctance (smaller flux linkage). With respect to an $\alpha\beta$ stationary reference frame, where the $\alpha$-axis is superimposed to the phase $a$-axis of phase $a$ and the $\beta$-axis is in quadrature to $\alpha$, the angle between the $d$-axis and the $\alpha$-axis is defined as the mechanical angle $\vartheta_{\mathrm{m}}$. In case of multiple pole pairs, for each mechanical rotation, multiple electrical rotations of the $dq$ reference frame occur. The number of rotations is equal to the pole pairs of the machine, with the relation $\vartheta_{\mathrm{me}} = p\vartheta_{\mathrm{m}}$, where $\vartheta_{\mathrm{me}}$ is the electromechanical angle and $p$ is the pole pair value.

The dynamic equations of the voltages and the currents in a stator with sinusoidally distributed three-phase windings can be written either for the $\alpha\beta$ or for the $dq$ reference frame. The $\alpha\beta$ reference frame equations are the following

$$\begin{aligned} u_{\mathrm{s}\alpha} &= R_{\mathrm{s}} i_{\mathrm{s}\alpha} + \frac{\mathrm{d}\lambda_{\mathrm{s}\alpha}}{\mathrm{d}t} \\ u_{\mathrm{s}\beta} &= R_{\mathrm{s}} i_{\mathrm{s}\beta} + \frac{\mathrm{d}\lambda_{\mathrm{s}\beta}}{\mathrm{d}t} \end{aligned} \tag{1}$$

where $R_{\mathrm{s}}$ is the stator resistance, $u_{\mathrm{s}\alpha}$ and $u_{\mathrm{s}\beta}$ are the stator voltages, $i_{\mathrm{s}\alpha}$ and $i_{\mathrm{s}\beta}$ are the stator currents, and $\lambda_{\mathrm{s}\alpha}$ and $\lambda_{\mathrm{s}\beta}$ are the stator flux linkages. An algebraic transformation in the rotating $dq$ reference frame is performed to obtain the following set of voltage balance equations

$$\begin{aligned} u_{\mathrm{s}d} &= R_{\mathrm{s}} i_{\mathrm{s}d} + \frac{\mathrm{d}\lambda_{\mathrm{s}d}}{\mathrm{d}t} - \omega_{\mathrm{me}}\lambda_{\mathrm{s}q} = R_{\mathrm{s}} i_{\mathrm{s}d} + \frac{\mathrm{d}\lambda_{\mathrm{s}d}}{\mathrm{d}t} + \mathrm{e}_{\mathrm{s}d} \\ u_{\mathrm{s}q} &= R_{\mathrm{s}} i_{\mathrm{s}q} + \frac{\mathrm{d}\lambda_{\mathrm{s}q}}{\mathrm{d}t} + \omega_{\mathrm{me}}\lambda_{\mathrm{s}d} = R_{\mathrm{s}} i_{\mathrm{s}q} + \frac{\mathrm{d}\lambda_{\mathrm{s}q}}{\mathrm{d}t} + \mathrm{e}_{\mathrm{s}q} \end{aligned} \tag{2}$$

where $u_{\mathrm{s}d}$ and $u_{\mathrm{s}q}$ are the stator voltages, $i_{\mathrm{s}d}$ and $i_{\mathrm{s}q}$ are the stator currents, $\lambda_{\mathrm{s}d}$ and $\lambda_{\mathrm{s}q}$ are the stator flux linkages and $\omega_{\mathrm{me}}$ is the electromechanical speed. The presence of the cross-coupling terms $e_{\mathrm{s}d}$ and $e_{\mathrm{s}q}$ is undesirable because of the coupling between the $d$-and $q$-axis.

On the basis of (2), the torque produced in the electromechanical conversion process is equal to

$$\tau = \frac{3}{2} p \left( \lambda_{\mathrm{s}d} i_{\mathrm{s}q} - \lambda_{\mathrm{s}q} i_{\mathrm{s}d} \right) \tag{3}$$

The torque is further used to complete the overall mechanical description of the system, with the following expression

$$\tau = J_{\mathrm{m}} \frac{\mathrm{d}\omega_{\mathrm{m}}}{\mathrm{d}t} + B_{\mathrm{m}} \omega_{\mathrm{m}} + \tau_{\mathrm{L}} \tag{4}$$

where $J_{\mathrm{m}}$ is the mechanical inertia, $B_{\mathrm{m}}$ is the viscous friction, $\omega_{\mathrm{m}}$ is the mechanical speed (with the relation $\omega_{\mathrm{me}} = p\omega_{\mathrm{m}}$) and $\tau_{\mathrm{L}}$ is the load torque.

So far, no assumption was made with regard to the nature of the magnetic circuit in the machine. As a matter of fact, (1) and (2) maintain their general validity for the description of a SynRM electromechanical conversion model, inclusive of copper loss but without any core losses contribution. A first approximation of (2) occurs when the magnetic circuit is considered to be linear. In this case, two inductances $L_{\mathrm{s}d}$ and $L_{\mathrm{s}q}$ are introduced, each of them defining the synchronous inductance in the $d$- or $q$-axis. With this assumption, the flux linkages $\lambda_{\mathrm{s}d}$ and $\lambda_{\mathrm{s}q}$ and thus the voltage balance equations are transformed as below

$$\begin{aligned} \lambda_{\mathrm{s}d} &= L_{\mathrm{s}d} i_{\mathrm{s}d} \\ \lambda_{\mathrm{s}q} &= L_{\mathrm{s}q} i_{\mathrm{s}q} \\ u_{\mathrm{s}d} &= R_{\mathrm{s}} i_{\mathrm{s}d} + L_{\mathrm{s}d} \frac{\mathrm{d}i_{\mathrm{s}d}}{\mathrm{d}t} - \omega_{\mathrm{me}} L_{\mathrm{s}q} i_{\mathrm{s}q} \\ u_{\mathrm{s}q} &= R_{\mathrm{s}} i_{\mathrm{s}q} + L_{\mathrm{s}q} \frac{\mathrm{d}i_{\mathrm{s}q}}{\mathrm{d}t} + \omega_{\mathrm{me}} L_{\mathrm{s}d} i_{\mathrm{s}d} \end{aligned} \tag{5}$$

It is worth noting that neither the $d$- nor the $q$-axis fluxes in (5) contain a flux contribution from permanent magnets, since a SynRM is considered in this work. However, the set of equations can be easily extended to the case of permanent-magnet-assisted SynRMs (PMaSynRMs), surface permanent magnet synchronous machines (SPM-SMs) or IPM-SMs. In the presence of magnets, the $dq$-axis definition introduced in this work could be revisited, for example by placing the $d$-axis in the direction of the flux produced by the magnets.

It is well known that the assumption of a linear magnetic circuit is a highly approximated one, especially when dealing with SynRMs, PMaSynRMs and IPM-SMs [1, 3]. The phenomena of magnetic saturation affect the magnetic circuit, rendering impossible to use constant inductance values in the model. Furthermore, the presence of the cross-magnetisation effects must be taken into account. Thus, the flux linkage cannot be modelled by means of a single-variable-dependent function as $\lambda_{\mathrm{s}d} = f_d(i_{\mathrm{s}d})$ or $\lambda_{\mathrm{s}q} = f_q(i_{\mathrm{s}q})$. In fact, each of the flux linkages $\lambda_{\mathrm{s}d}$ or $\lambda_{\mathrm{s}q}$ is dependent on both $i_{\mathrm{s}d}$ and $i_{\mathrm{s}q}$ at the same time, thus establishing the following general relation

$$\begin{aligned} \lambda_{\mathrm{s}d} &= f_d\left(i_{\mathrm{s}d}, i_{\mathrm{s}q}\right) \\ \lambda_{\mathrm{s}q} &= f_q\left(i_{\mathrm{s}d}, i_{\mathrm{s}q}\right) \end{aligned} \tag{6}$$

When synchronous machines exhibit magnetic saturation and cross-magnetisation effects, the concept of inductance as introduced in (5) does not hold any more, requiring a re-definition. Two different alternatives exist. In the first one, the SynRM model is kept at the general level defined in (2), thus using only the flux linkage curves without introducing any inductance definition. The second approach, instead, might be used for control approaches where a more familiar inductance representation is beneficial, for the easiness of the mathematical formulation. Examples are represented by high-frequency position-sensorless control approaches, as in [29]. In this case, two new inductance definitions can be introduced: the apparent inductance and the differential inductance. Given an operating point of the SynRM currents

$(i_{sd_0}, i_{sq_0})$, the apparent inductances are defined as follows

$$L_{sda}\left(i_{sd_0}, i_{sq_0}\right) = \frac{\lambda_{sd}\left(i_{sd_0}, i_{sq_0}\right)}{i_{sd_0}}$$
$$L_{sqa}\left(i_{sd_0}, i_{sq_0}\right) = \frac{\lambda_{sq}\left(i_{sd_0}, i_{sq_0}\right)}{i_{sq_0}} \quad (7)$$

According to the definition in (7), the apparent inductances represent the ratio between the flux linkage and the corresponding current on the same axis, specified for the given operating point. The apparent inductances carry the information on the magnetic flux level of the machine in the operating point described by the pair $(i_{sd_0}, i_{sq_0})$, and therefore they are used for large-signal representations of the SynRM electromagnetic circuit. The differential inductances, instead, are defined as

$$L_{sdd}\left(i_{sd_0}, i_{sq_0}\right) = \frac{\partial\lambda_{sd}\left(i_{sd_0}, i_{sq_0}\right)}{\partial i_{sd}}$$
$$L_{sdq}\left(i_{sd_0}, i_{sq_0}\right) = \frac{\partial\lambda_{sd}\left(i_{sd_0}, i_{sq_0}\right)}{\partial i_{sq}}$$
$$L_{sqd}\left(i_{sd_0}, i_{sq_0}\right) = \frac{\partial\lambda_{sq}\left(i_{sd_0}, i_{sq_0}\right)}{\partial i_{sd}}$$
$$L_{sqq}\left(i_{sd_0}, i_{sq_0}\right) = \frac{\partial\lambda_{sq}\left(i_{sd_0}, i_{sq_0}\right)}{\partial i_{sq}} \quad (8)$$

From (8) it follows that the differential inductances represent the slope of the surface plot of the flux linkage (either in the $d$- or in the $q$-axis) with respect to the two variables $i_{sd}$ or $i_{sq}$. They carry the information on the small-signal behaviour of the magnetic circuit.

Fig. 1*a* reports the equivalent large-signal representation of the SynRM electrical circuit, based on (2) and (7). The circuit is reported only for the $d$-axis, while the equivalent $q$-axis representation can be obtained in the same manner. A similar circuit can be drawn for the small-signal case, using (2) and (8) and by substituting $L_{sda}$ with $L_{sdd}$ in Fig. 1*a*. When a standstill condition is achieved, the electromechanical speed is zero and thus the same circuit can be used by setting $e_{sd} = 0$. The standstill condition will be considered while describing the self-commissioning methods in Section 3.

An important consideration refers to the details of the machine model considered so far. The equations in (2) and the circuit in Fig. 1*a* include an electromechanical conversion model with copper loss, but do not consider the modelling of core losses caused by hysteresis and eddy currents. In some cases, the contribution of core loss to the overall dynamic behaviour of the machines is very small and thus neglected. However, as described from Section 3 onwards, the contribution of core losses cannot be neglected in this work. For this reason, the circuit of Fig. 1*a* is modified according to the conventional core loss models available in the literature (see [14] for a description of the series or parallel model in a permanent magnet synchronous machine), where an equivalent variable resistance is introduced to take into account the core losses effect. The modified circuit is reported in Fig. 1*b*.

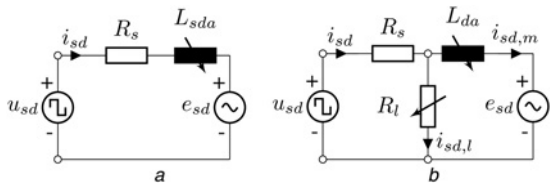


**Fig. 1** *SynRM large-signals d-axis equivalent circuit*
*a* With copper losses only
*b* With copper losses and core losses

## 3 Self-commissioning procedure

### 3.1 Non-standstill estimation of flux linkage curves

Different approaches for the estimation of the flux linkage curves can be obtained directly from (2). Assuming that the machine is rotating in a steady-state condition in the $dq$ reference frame, the flux derivatives in (2) disappear and the fluxes can be obtained as

$$\lambda_{sd} = \frac{u_{sq} - R_s i_{sq}}{\omega_{me}}$$
$$\lambda_{sq} = -\frac{u_{sd} - R_s i_{sd}}{\omega_{me}} \quad (9)$$

This approach is used by Armando *et al.* [1], Pellegrino *et al.* [2], Cintron-Rivera *et al.* [3]. It is not meant to be a standstill self-commissioning method, as it requires a speed-controlled load machine to keep the speed constant or a freely rotating rotor disconnected from any sensitive load, while the machine under test is controlled in different operating points of the currents $(i_{sd}, i_{sq})$. However, these methods are known for the reliability of the estimated flux linkage tables, to which the results of other self-commissioning procedures can be compared with.

### 3.2 Previous methods based on differential inductance estimation

The main idea behind a standstill or a quasi-standstill condition is that the terms dependent on $\omega_{me}$ in (2) can be neglected. To achieve this advantageous condition, solutions given by Peretti and Svechkarenko [25], Odhano *et al.* [26], Odhano *et al.* [27], Wang *et al.* [28] keep one current (eg. $i_{sd}$) at a constant DC level, while the other one (eg. $i_{sq}$) is controlled with a square-wave reference. The square-wave frequency is high enough to produce an oscillating torque which is filtered out by the mechanical system, returning a zero or almost-zero speed condition. In this way, the use of the circuit in Fig. 1 with $e_{sd} = 0$ is allowed.

Peretti and Svechkarenko [25], Odhano *et al.* [26], Odhano *et al.* [27], Wang *et al.* [28] use a small-signal injection on the top of the imposed references to estimate the differential inductances, and then obtain the flux linkage curves by integration of the estimated differential inductances over the current range, according to the definitions reported in (8). The small-signal injection can be performed either as a voltage injection or as a current injection.

The DC amplitude level on the $d$-axis and the square-wave amplitude on the $q$-axis allow for a complete exploration of the flux linkages for the desired operating points of the currents $(i_{sd}, i_{sq})$. In principle, the square-wave reference could be applied to the $d$-axis and the DC reference to the $q$-axis, obtaining a similar torque with zero mean value. The best choice is the one that requires less voltage, that is the square-wave reference should be selected for the axis with the highest magnetic reluctance (smallest inductance).

The estimation of the differential inductances needs to record the injected voltage pattern and the oscillation of the currents at the injected frequency. A standstill evaluation of the impedance of the SynRM circuit can be obtained using the circuit representation of Fig. 1*a*, described for small-signal injection. The differential inductance can be calculated by considering the imaginary part of the measured impedance [26]. However, when the core losses equivalent resistance of Fig. 1*b* is neglected, the estimation of the differential inductance based on the values of $i_{sd}$ or $i_{sq}$ (which are the only available measurements in an inverter) could potentially lead to incorrect results, depending on the value of $R_l$ in Fig. 1*b*.

This is caused by the inherent approximation $i_{sd} \simeq i_{sd,\mathrm{m}}$, which could not be verified for all cases. As a matter of fact $|i_{sd}| > |i_{sd,\mathrm{m}}|$, and this leads to underestimated differential inductances. This systematic error has been described without proposing a solution in [29]. An evidence of this problem will be shown in Section 4.3.

### 3.3 Proposed self-commissioning method

The proposed methodology works with the same control scheme and the same combination of constant/square-wave current references described in Section 3.2, but does not apply any small-signal injection. Instead, the flux linkages are estimated from (2) with an integral operation

$$\lambda_{sd} = \int \left(u_{sd} - R_s i_{sd}\right) \mathrm{d}t$$
$$\lambda_{sq} = \int \left(u_{sq} - R_s i_{sq}\right) \mathrm{d}t \tag{10}$$

On the basis of (10), Fig. 2 shows the schematic of the proposed self-commissioning procedure.

The flux estimation through (10) is still valid when the resistance $R_l$ in Fig. 1*b* is taken into account. The integration in (10) returns the magnetic flux in the inductor (whose value in different operating points is the scope of this work), without posing any assumption on the core losses, as long as the standstill or quasi-standstill condition is kept. Four aspects are worth to underline:

- The integration must reach a steady-state condition in order to bypass the effect of hysteresis, as it has been observed and reported later in Section 4.3. This means that the square-wave reference current cannot be substituted by a sinusoidal reference.
- Only the flux linkage values at the end of the transient are considered as valid, as shown by the circles around the $\lambda_{sd}$ profile in Fig. 2. This choice is again related to the avoidance of hysteresis effects.
- The estimation of the $\lambda_{sd}$ is obtained with square-wave current references for $i_{sd}$ and constant references for $i_{sq}$, while the estimation of $\lambda_{sq}$ is obtained with square-wave current references for $i_{sq}$ and constant references for $i_{sd}$. This means that the square-wave references must be applied also to the axis with lower magnetic reluctance (largest inductance).
- The digital integration must be performed with offset-free inputs, which means that the recorded voltages and currents must be cleaned from their (induced or spurious) average value. This operation is not difficult to perform, once a few square-wave periods have been recorded.

## 4 Experimental measurements

### 4.1 Experimental setup

A picture of the test bench used for the experiments is reported in Fig. 3. The 11 kW SynRM prototype under test, whose parameters are reported in Table 1 in the Appendix, is shown on the right side of the picture. The load machine (an 11 kW Baldor machine) is visible on the left side. The load machine is controlled via an off-the-shelf ABB ACS850. The SynRM, instead, is connected only to the power unit of an ABB ACS850, while its control board has been replaced by a custom interface and connected to an OPAL-RT Technologies OP5600 system (the black box on the left upper side of the figure). The OP5600 is equipped with a quad-core Intel DSP processor at 2.4 GHz and a Virtex 6 FPGA. The phase currents and the DC-bus voltage are measured with a custom measurement box (the grey box behind the load machine) and connected to the A/D board of the OP5600. The digital I/O of the OP5600 is used to communicate with the ACS850 power unit through the custom interface. The phase voltage values which are required to perform the integration in (10) are obtained by estimation, compensating the inverter non-linearities with

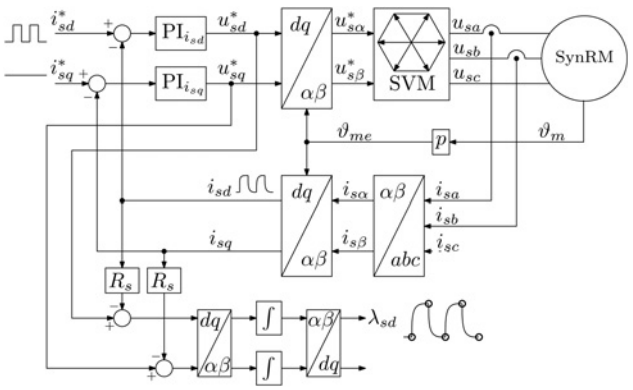


**Fig. 2** *General schematic of the proposed self-commissioning method*

conventional methods as in [30], and using the imposed reference voltages instead.

### 4.2 Generation of the flux linkage reference curves

The preliminary experiments were aimed at generating reliable curves for the flux linkages, by using the methods described in Section 3.1. A speed-regulated load machine was used to keep the SynRM under test at a constant rotating speed of 200 rpm, for an electrical frequency of 6.67 Hz. The frequency was considered low enough to neglect the effect of core losses in the definition of the reference curves. The obtained maps are shown in Fig. 4, serving as reference curves for the test of the proposed self-commissioning method.

### 4.3 Experimental measurements highlighting the presence of core loss effects

The method based on small-signal injection and differential inductance estimation described in Section 3.2 was tested first. A small-signal sinusoidal voltage injection was used, while keeping a constant current reference for $i_{sd}$ with $i_{sq} = 0$ A. The voltage injection amplitude was selected in order to obtain the same amplitude of the oscillating current, despite the change in frequency. The differential inductance was calculated via the impedance calculation, after recording the oscillating voltage and current. This operating point was chosen for its simplicity and the absence of oscillating torque, which might have caused a difficult interpretation of the results. The obtained graphs are shown in

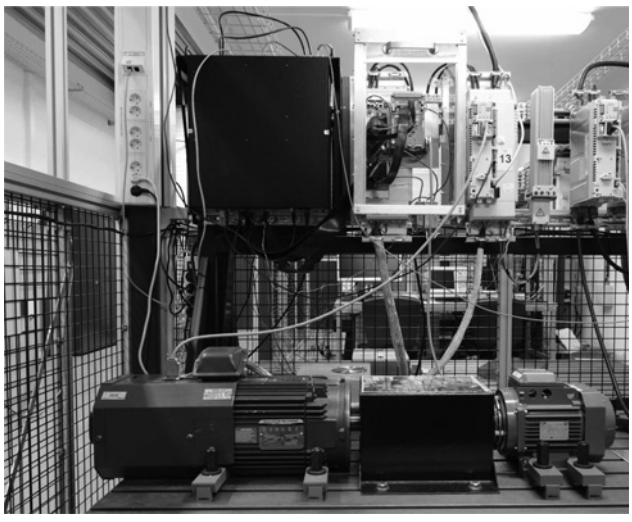

**Fig. 3** *Experimental setup*

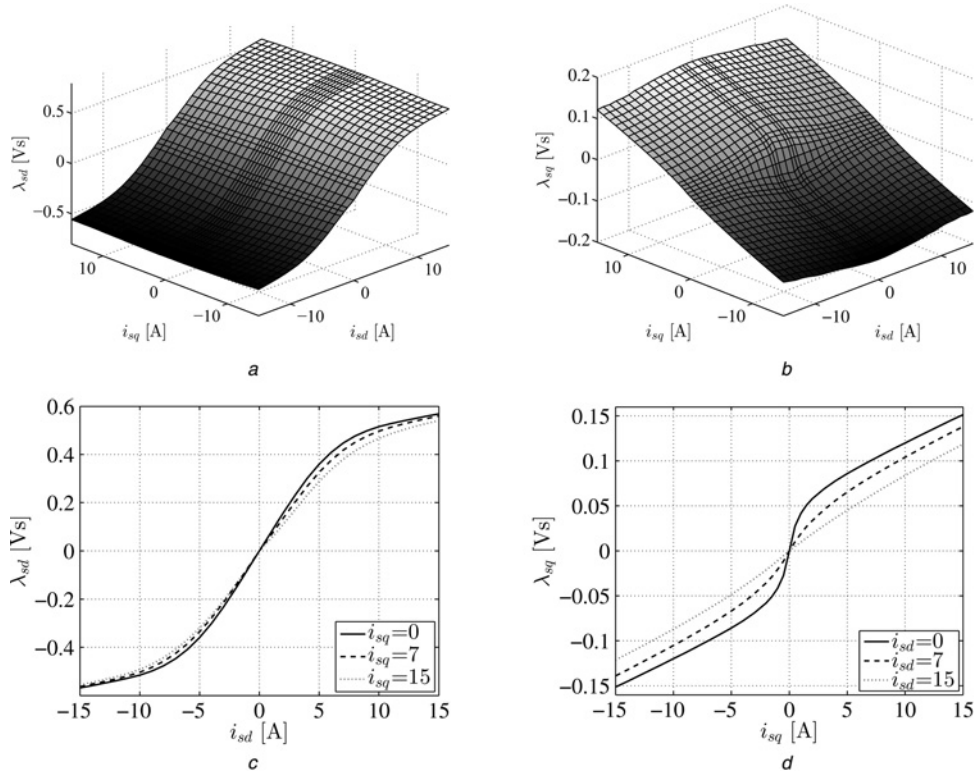


**Fig. 4** *Experimental flux linkage reference curves for the SynRM under test*

*a* $\lambda_{sd} = f_d(i_{sd}, i_{sq})$
*b* $\lambda_{sq} = f_q(i_{sd}, i_{sq})$
*c* One-dimensional plot of $\lambda_{sd}$ for few $i_{sq}$ values
*d* One-dimensional plot of $\lambda_{sq}$ for few $i_{sd}$ values

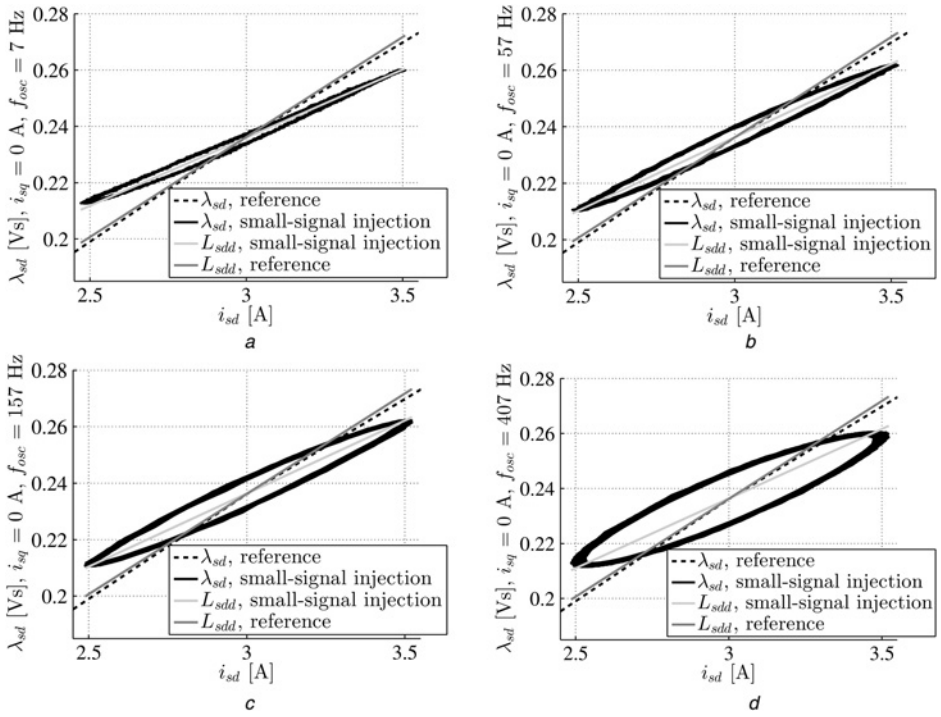


**Fig. 5** *Small-signal current injection for $L_{sdd}$ estimation with varying frequency*

*a* 7 Hz injection
*b* 57 Hz injection
*c* 157 Hz injection
*d* 407 Hz injection

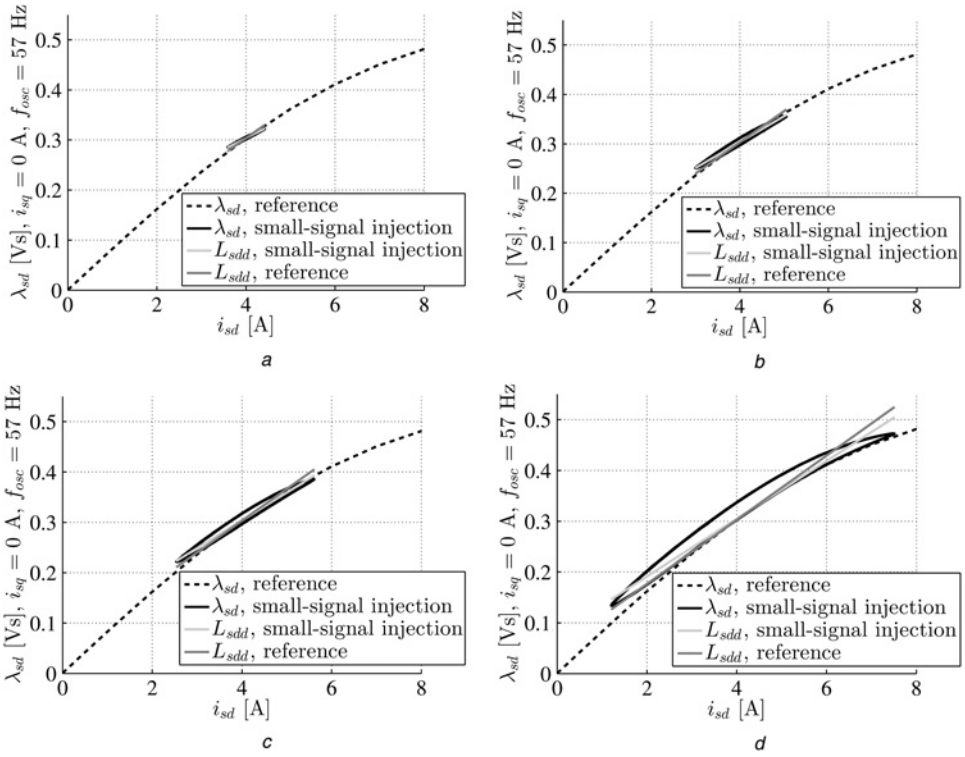


**Fig. 6** *$L_{sdd}$ estimation with small-signal voltage injection at 57 Hz and varying amplitude*

*a* 6.5 V
*b* 18.8 V
*c* 29.5 V
*d* 61.0 V

Fig. 5 for four different frequencies of injection (7, 57, 157 and 407 Hz). The flux linkage reference curve and its reference differential inductance (indicated in Fig. 5 as the tangent of the flux curve) are superimposed to the small-signal flux loop, which was obtained by means of an integration of the voltage minus the stator resistance voltage drop.

The measurements indicate that the estimated differential inductance is directed on the major axis of the resulting ellipse, and always lower than the value obtained from the reference flux linkage curve. The elliptic profile of the flux around the operating point indicates the presence of other elements in the circuit of Fig. 1*a*, and possibly the presence of other non-linear local phenomena as, for example, Rayleigh loops (as reported in [31]). It is worth to underline the growing width of the ellipsoid as a function of the frequency, which adds to the fact that the ellipse is swept faster for increasing frequencies. This indicates a more-than-linear dependence of the losses with the frequency.

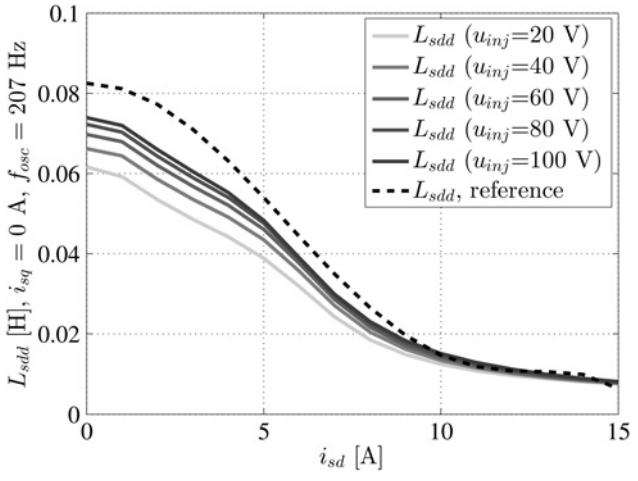


**Fig. 7** *Differential inductance estimation with increasing injected voltage magnitude*

A second batch of measurements was performed with a sinusoidal voltage injection at a constant frequency of 57 Hz and increasing amplitude. The results are shown in Fig. 6. Again, the estimated differential inductance is always lower than the reference one. A notable phenomenon is the distortion of the ellipsoid for higher amplitudes of the injected voltage, indicating that the system cannot be modelled with small-signal circuits any longer.

Although an increase of voltage injection amplitude seemed to reduce the error of the differential inductance estimation (from almost 30% error in Fig. 6*a* to 10% error in Fig. 6*d*), it was found that large increases did not bring any estimation benefits. This phenomenon is shown in Fig. 7 where the estimated differential inductance curves are getting closer to each other for increased injected voltage amplitudes (indicated as $|u_{\text{inj}}|$). Besides, this practice goes against the concept of small-signal injection itself. An interesting aspect is the convergence of all estimated differential inductances to the reference inductance for high-current values.

### 4.4 Tests on the proposed self-commissioning procedure

The approach proposed in Section 3.3 was verified as follows. First, the curves of $\lambda_{sd}$ for $i_{sq} = 0$ and of $\lambda_{sq}$ for $i_{sd} = 0$ were evaluated, thus without producing any torque. After the first two curves were generated, the differential inductances $L_{sdd}$ and $L_{sqq}$ were calculated. Based on their values, the proportional-integral (PI) regulators in Fig. 2 were tuned with a pole-cancellation method, where the zero of the PI transfer function was tuned at the pole of the $i_{sd}/u_{sd}$ or the $i_{sq}/u_{sq}$ transfer function. Thus, the PI regulators were tuned with adaptive parameters depending on $i_{sd}$ and $i_{sq}$. This choice was made in order to maintain a similar current regulation

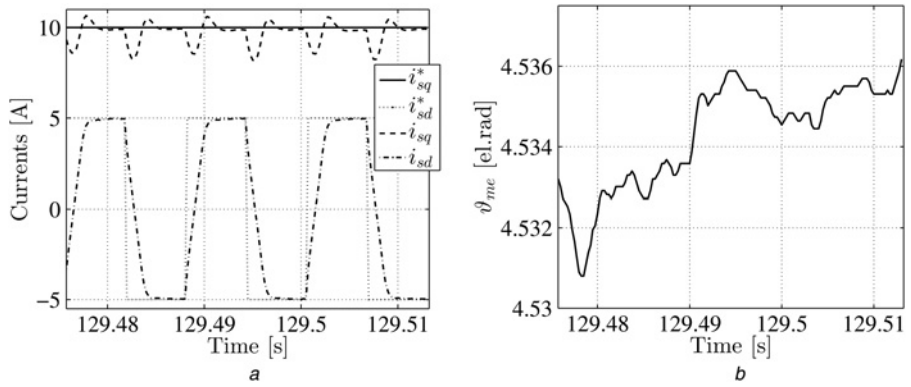


**Fig. 8** *Typical time-domain profile of*
*a* $i_{sd}$ and $i_{sq}$
*b* $\vartheta_{me}$

dynamics over the whole range of currents, although it is not strictly necessary. The method of Fig. 2 was subsequently applied for different operating points of the currents ($i_{sd}$, $i_{sq}$), where the square-wave references had a frequency of 80 Hz. The frequency was high enough to consider the system in a quasi-standstill condition. It is worth to note that the choice of non-adaptive PI parameters would have led to reduced current dynamics in some operating points, forcing a selection of a lower square-wave frequency and thus weakening the quasi-standstill condition. Moreover, for a better precision of the integrals in (10), the value of $R_s$ was recalculated at each square wave period, by averaging the values of voltages and currents in the time domain during their short steady-state interval. A typical time-domain profile of the currents and of the position is reported in Fig. 8, showing that despite the variation of the currents, the rotor movement was negligible. The $i_{sq}$ variations are caused by two effects: one is the presence of small-rotor vibrations inducing a coupling effect between the $d$-and the $q$-axis according to (2), since the electrical speed is not completely zero. The second effect is correlated with the derivative of the flux linkages that are dependent on both currents independently from the value of the electrical speed, as shown by (2), (6) and (8). Thus, any variation of the current/flux on one axis has a direct effect on the other axis too, through $L_{sdq}$ and $L_{sqd}$ in (8). In any case, the small $i_{sq}$ variations did not cause any problem during the data collection process, because the flux linkage maps were created by considering only the latest samples

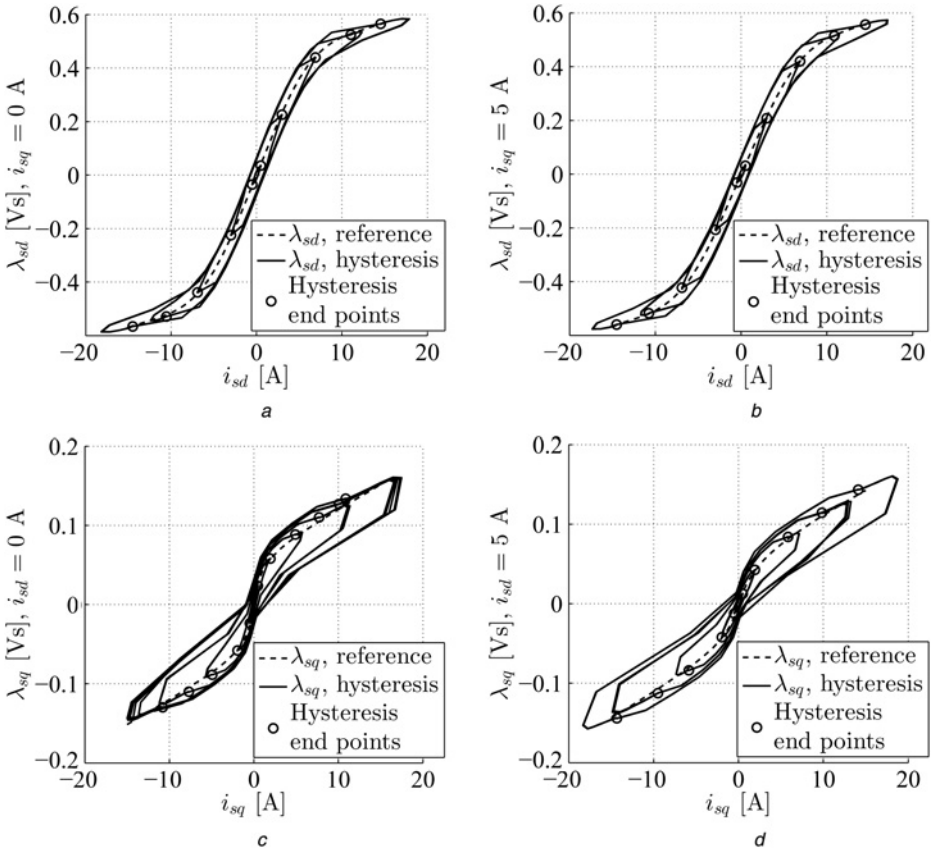


**Fig. 9** *Connection of the hysteresis vertex in the proposed method*

*a* $\lambda_{sd}$ curve for $i_{sq} = 0$ A
*b* $\lambda_{sd}$ curve for $i_{sq} = 5$ A
*c* $\lambda_{sq}$ curve for $i_{sd} = 0$ A
*d* $\lambda_{sq}$ curve for $i_{sd} = 5$ A

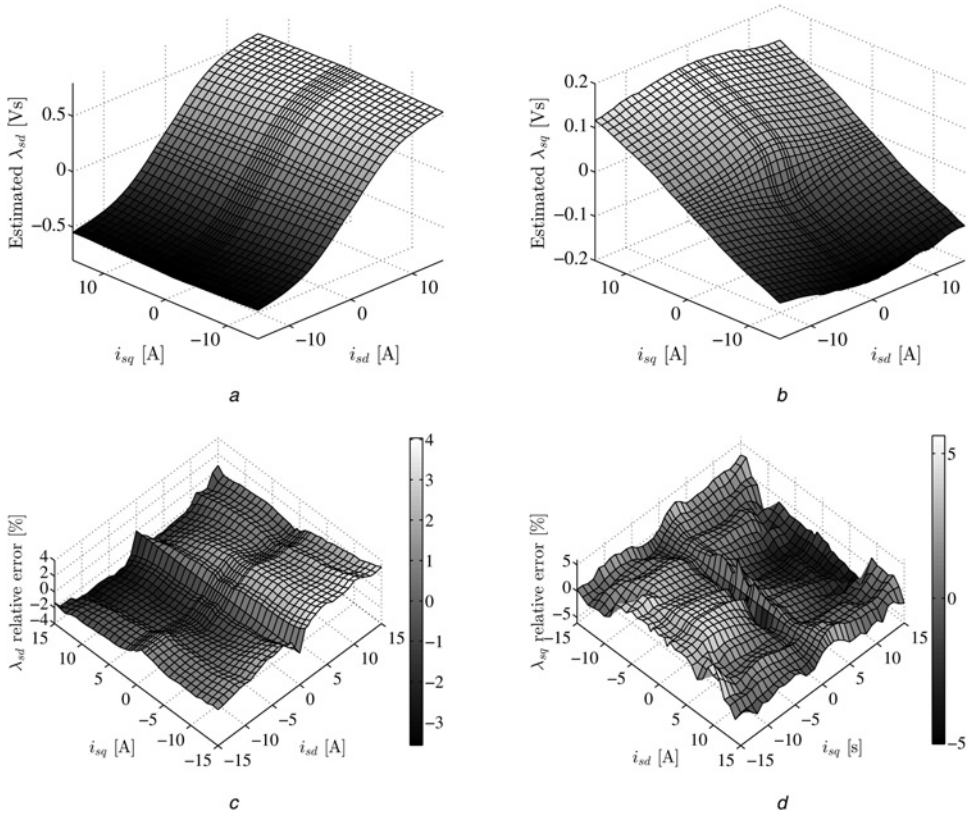


**Fig. 10** *Estimated flux linkage curves with the proposed method*

*a* $\lambda_{sd}$
*b* $\lambda_{sq}$
*c* Estimation error on the *d*-axis
*d* Estimation error on the *q*-axis

of $i_{sq}$ after the steady-state condition was reached. In the meanwhile, the integral on the *d*-axis was calculated over half period of the square-wave signal.

An important aspect regarding the magnitude of rotor vibrations is related to the inertia of the system under test. In this case, the quasi-standstill method benefits the back-to-back connection of the two motors and the torque meter in between them. Thus, the inertia is higher than the initial SynRM inertia, as documented in Table 1. However, it is believed that the bench is representative of a conventional plant installation where the motor cannot be disconnected from its mechanical load. This turns out to be a positive aspect for the proposed estimation method, due to the increased inertia of the system. When a motor is free to rotate, instead, quasi-standstill self-commissioning procedures are unlikely to be used, since other easier non-standstill estimation methods could be exploited instead, as the one in [2].

Fig. 9 reports the hysteresis cycles traced by the integrals of (10) for the selected square-wave reference magnitude of the oscillating current, for both *d*-and *q*-axis, in the case where the constant current is not equal to zero. The superposition of the flux linkage reference curve shows that by taking the end points of the hysteresis cycles, the flux curve can be reconstructed with a reduced error. It is worth underlying that the end points of the hysteresis cycles are not necessarily the vertices of the loops, as the trajectory of the flux in a hysteresis cycle depends on the current transient. In the case of Fig. 9, the current dynamics is affected by the tuning of the current PI regulators. Although the PIs are tuned adaptively based on the curves when $i_{sd}$ (or $i_{sq}$) is zero and $i_{sq}$ (or $i_{sd}$) is set over the whole nominal range, the tuning is not perfect for all operating points, especially when cross-magnetising currents are present. Thus, the current and flux transients might present slight overshoots before settling to a steady end point. These end points, marked in Fig. 9, are the ones to consider when estimating the flux curves.

A comparison of the estimated flux linkage maps of the proposed method, with respect to the reference flux linkage maps of Fig. 4, is reported in Fig. 10. Figs. 10*a* and *b* report the estimated flux linkage curves, while Figs. 10*c* and *d* show the estimation error, relative to the maximum flux in the curves of Fig. 4. The error is kept within ± 5% for the complete range of the currents, without any constant bias. Slightly larger errors are measured for $\lambda_{sq}$, probably due to the smaller voltages measured during the square-wave transients, which might induce more error in the presence of an imperfect compensation of the inverter non-linearities. Other sources of estimation errors might be related to the non-perfect steady-state condition reached by the currents following the square-wave references, and to spurious effects related to the quasi-standstill condition with a non-perfect zero speed. It is also worth underlying that the estimation method was performed for one mechanical position only, since a standstill (or quasi-standstill) condition was sought. The possible variations of the flux linkage as a function of the rotor position (interaction between the rotor and the stator slots) are therefore not taken into account. In principle, especially for machines with significant position-dependant flux linkages, it is possible to repeat the proposed method for different rotor positions, adding one more input variable to the flux linkage maps ($i_{sd}$, $i_{sq}$ and $\vartheta_{\mathrm{me}}$). This aspect will anyway lead to a non-standstill condition. Nevertheless, considering the outcome of the estimation of this case, the results for both axes are considered more than satisfactory.

### 4.5 Comparison with other estimation methods

Among other methods for estimating the flux linkages, two solutions were tested. The first one is described in [7–9], where the flux linkage curve is estimated by averaging the lower and the higher trajectories of the hysteresis loop. Fig. 11 reports the estimation

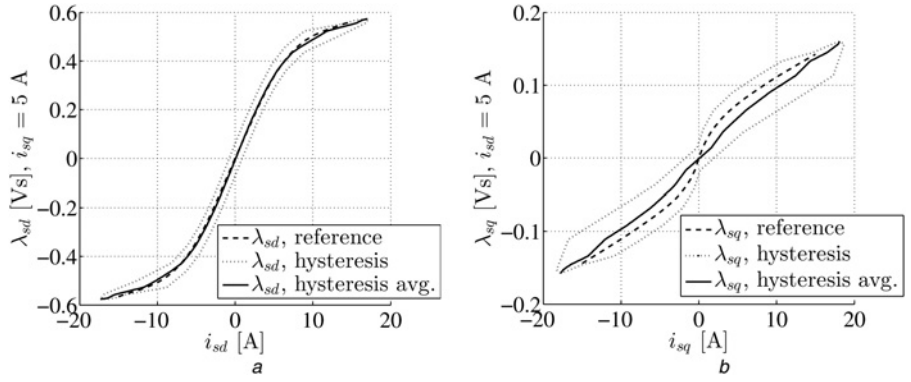


**Fig. 11** *One-hysteresis average method*

*a* $\lambda_{sd}$ curve for $i_{sq} = 5$ A
*b* $\lambda_{sq}$ curve for $i_{sd} = 5$ A

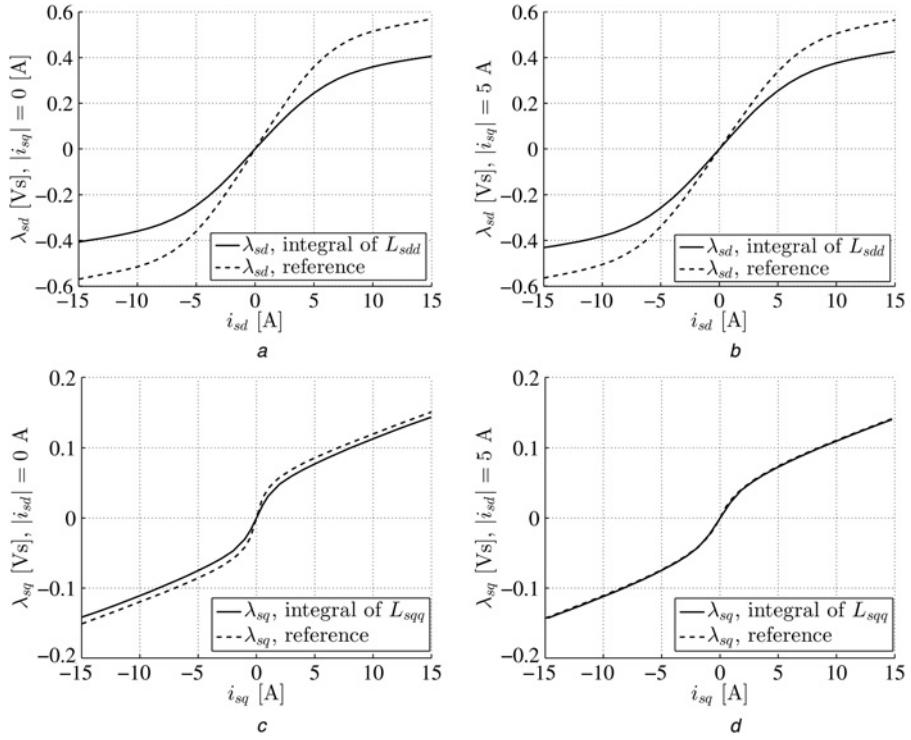


**Fig. 12** *Differential-inductance-based method*

*a* $\lambda_{sd}$ curve for $|i_{sq}| = 0$ A
*b* $\lambda_{sd}$ curve for $|i_{sq}| = 5$ A
*c* $\lambda_{sq}$ curve for $|i_{sd}| = 0$ A
*d* $\lambda_{sq}$ curve for $|i_{sd}| = 5$ A

for $\lambda_{sd}$ and $\lambda_{sq}$ for a non-zero cross-magnetising current. The approach seems to induce some estimation deviations for the SynRM under investigation especially for $\lambda_{sq}$. The deviation could be related to the asymmetric hysteresis cycles of $\lambda_{sq}$ visible in Fig. 9*d*. This asymmetry might be caused by the quasi-standstill condition, in addition to the inherent difficulty of estimating $\lambda_{sq}$ because of the lower voltage values involved in the transients.

The second estimation method was taken from any of the solutions presented in [25, 26] or [27], and it was based on a small-signal injection at 307 Hz with differential inductance estimation. Fig. 12 reports the estimation results. A large error is consistently present on the *d*-axis flux linkage estimation, whilst the *q*-axis estimate shows a smaller error. In general, both flux linkage estimations show reduced errors when in the presence of the cross-magnetising current component, in particular for the *q*-axis estimation (Figs. 12*b* and *d*).

## 5 Conclusions

A self-commissioning procedure for the estimation of flux linkage curves in SynRMs was proposed. The procedure is capable of estimating the curves at standstill (when either $i_{sd}$ or $i_{sq}$ is equal to zero) and at quasi-standstill condition (when both currents are different from zero), by applying a combination of constant and square-wave current patterns without small-signal injection, and calculating the flux by means of an integral operation. The proposed approach bypasses the issue of unmodelled core losses, which causes some estimation deviations in small-signal injection methods that estimate the differential inductances. Evidence of the impact of the core losses on the flux linkage estimation is produced, and experimental tests of the proposed procedure show excellent agreement between the estimated flux linkage curves and the reference flux linkage curves obtained in laboratory.

## 6 Acknowledgment

The authors thank Dr. Dmitry Svechkarenko, ABB Corporate Research Västerås, Sweden, for his contribution in the definition of the signal injection method described in the patent [25].

## 7 References

1 Armando, E., Bojoi, R., Guglielmi, P., *et al.*: 'Experimental identification of the magnetic model of synchronous machines', *IEEE Trans. Ind. Appl.*, 2013, **49**, (5), pp. 2116–2125
2 Pellegrino, G., Boazzo, B., Jahns, T.M.: 'Magnetic model self-identification for PM synchronous machine drives', *IEEE Trans. Ind. Appl.*, 2015, **51**, (3), pp. 2246–2254
3 Cintron-Rivera, J.G., Babel, A.S., Montalvo-Ortiz, E.E., *et al.*: 'A simplified characterization method including saturation effects for permanent magnet machines'. Proc. of the XXth Int. Conf. on Electrical Machines (ICEM), Marseille, France, September 2–5 2012, pp. 837–843
4 Babel, A.S., Cintron-Rivera, J.G., Foster, S.N., *et al.*: 'Evaluation of a parameter identification method for permanent magnet AC machines through parametric sensitivity analysis', *IEEE Trans. Energy Convers.*, 2014, **29**, (1), pp. 240–249
5 Štumberger, B., Hamler, A., Hribernik, B.: 'Analysis of iron loss in interior permanent magnet synchronous motor over a wide-speed range of constant output power operation', *IEEE Trans. Magn.*, 2000, **36**, (4), pp. 1846–1849
6 Štumberger, G., Štumberger, B., Dolinar, D., *et al.*: 'Cross magnetization effect on inductances of linear synchronous reluctance motor under load conditions', *IEEE Trans. Magn.*, 2001, **37**, (5), pp. 3658–3662
7 Štumberger, B., Štumberger, G., Dolinar, D., *et al.*: 'Evaluation of saturation and cross-magnetization effects in interior permanent-magnet synchronous motor', *IEEE Trans. Ind. Appl.*, 2003, **39**, (5), pp. 698–709
8 Štumberger, G., Štumberger, B., Dolinar, D.: 'Identification of linear synchronous reluctance motor parameters', *IEEE Trans. Ind. Appl.*, 2004, **40**, (5), pp. 1317–1324
9 Štumberger, G., Polajžer, B., Štumberger, B., *et al.*: 'Evaluation of experimental methods for determining the magnetically nonlinear characteristics of electromagnetic devices', *IEEE Trans. Magn.*, 2005, **41**, (10), pp. 4030–4032
10 Štumberger, G., Marčič, T., Štumberger, B., *et al.*: 'Experimental method for determining magnetically nonlinear characteristics of electric machines with magnetically nonlinear and anisotropic iron core, damping windings and permanent magnets', *IEEE Trans. Magn.*, 2008, **44**, (11), pp. 4341–4344
11 Marčič, T., Štumberger, G., Štumberger, B.: 'Analyzing the magnetic flux linkage characteristics of alternating current rotating machines by experimental method', *IEEE Trans. Magn.*, 2011, **47**, (9), pp. 2283–2291
12 Levi, E., Sokola, M., Boglietti, A., *et al.*: 'Iron loss in rotor-flux-oriented induction machines: identification, assessment of detuning, and compensation', *IEEE Trans. Power Electron.*, 1996, **11**, (5), pp. 698–709
13 Dittrich, A.: 'Model based identification of the iron loss resistance of an induction machine'. Seventh Int. Conf. on Power Electronics and Variable Speed Drives (Conf. Publ. No. 456), London, UK, September 21–23 1998, vol. 3, pp. 500–503
14 Urasaki, N., Senjyu, T., Uezato, K.: 'Relationship of parallel model and series model for PMSM including iron loss'. Proc. of the IEEE 32nd Annual Power Electronics Specialists Conf. (PESC), Vancouver, BC, Canada, June 17–21 2001, vol. 2, pp. 788–793
15 Senjyu, T., Kinjo, K., Urasaki, N., *et al.*: 'Parameter measurement for PMSM using adaptive identification'. Proc. of the 2002 IEEE Int. Symp. on Industrial Electronics (ISIE), L'Aquila, Italy, July 7–11 2002, vol. 3, pp. 711–716
16 Urasaki, N., Senjyu, T., Uezato, K.: 'A novel calculation method for iron loss resistance suitable in modeling permanent-magnet synchronous motors', *IEEE Trans. Energy Convers.*, 2003, **18**, (1), pp. 41–47
17 Lar, I., Radulescu, M.M.: 'Equivalent core-loss resistance identification for interior permanent-magnet synchronous machines'. Proc. of the XXth Int. Conf. on Electrical Machines (ICEM), Marseille, France, September 2–5 2012, pp. 1667–1671
18 Boglietti, A., Cavagnino, A., Lazzari, M.: 'Experimental high-frequency parameter identification of AC electrical motors', *IEEE Trans. Ind. Appl.*, 2007, **43**, (1), pp. 23–29
19 Seilmeier, M., Ebersberger, S., Piepenbreier, B.: 'Identification of high frequency resistances and inductances for sensorless control of PMSM'. Proc. of the IEEE Int. Symp. on Sensorless Control for Electrical Drives and Predictive Control of Electrical Drives and Power Electronics (SLED/PRECEDE), Munich, Germany, October 17–19 2013, pp. 1–8
20 Wang, X., Xie, W.: 'Analysis of losses in a novel IPMSM resulting from high-frequency injection for sensorless control'. Proc. of the IEEE Int. Symp. on Sensorless Control for Electrical Drives and Predictive Control of Electrical Drives and Power Electronics (SLED/PRECEDE), Munich, Germany, October 17–19 2013, pp. 1–5
21 Alberti, L., Bianchi, N., Morandin, M., *et al.*: 'Analysis and tests of the sensorless rotor position detection of ringed-pole permanent-magnet motor', *IEEE Trans. Ind. Appl.*, 2014, **50**, (5), pp. 3278–3284
22 Alberti, L., Bianchi, N., Bolognani, S.: 'High frequency $d-q$ model of synchronous machines for sensorless control'. Proc. of Energy Conversion Congress and Exposition (ECCE 2014), Pittsburg, PA, USA, September 14–18 2014, pp. 4147–4153
23 Carraro, M., Tinazzi, F., Zigliotto, M.: 'Estimation of the direct-axis inductance in PM synchronous motor drives at standstill'. Proc. of the IEEE Int. Conf. on Industrial Technology (ICIT), Cape Town, South Africa, February 25–28 2013, pp. 313–318
24 Landsmann, P., Kennel, R.: 'Q-axis pulse based identification of the anisotropy displacement over load for surface mounted PMSM'. Proc. of the IEEE Int. Symp. on Sensorless Control for Electrical Drives and Predictive Control of Electrical Drives and Power Electronics (SLED/PRECEDE), Munich, Germany, October 17–19 2013, pp. 1–6
25 Peretti, L., Svechkarenko, D.: 'Self-commissioning procedure for inductance estimation in an electrical machine'. European Patent application EP2 555 420 A1, August 01, 2011, also available as WO2013017386 (A1), CN103650331 (A), US2014145655 (A1)
26 Odhano, S.A., Giangrande, P., Bojoi, R.I., *et al.*: 'Self-commissioning of interior permanent-magnet synchronous motor drives with high-frequency current injection', *IEEE Trans. Ind. Appl.*, 2014, **50**, (5), pp. 3295–3303
27 Odhano, S.A., Bojoi, R., Rosu, S.G., *et al.*: 'Identification of the magnetic model of permanent magnet synchronous machines using DC-biased low frequency AC signal injection'. Proc. of Energy Conversion Congress and Exposition (ECCE 2014), Pittsburg, PA, USA, September 14–18 2014, pp. 1722–1728
28 Wang, G., Qu, L., Zhan, H., *et al.*: 'Self-commissioning of permanent magnet synchronous machine drives at standstill considering inverter nonlinearities', *IEEE Trans. Power Electron.*, 2014, **29**, (12), pp. 6615–6627
29 Kuehl, S., Kennel, R.: 'Measuring magnetic properties of synchronous machines by applying angle estimation techniques known from sensorless control', *IEEE Trans. Ind. Appl.*, 2014, **50**, (6), pp. 3816–3824
30 Choi, J.-W., Sul, S.-K.: 'Inverter output voltage synthesis using novel dead time compensation', *IEEE Trans. Power Electron.*, 2006, **11**, (2), pp. 221–227
31 Cordier, J., Landsmann, P., Kennel, R.: 'The influence of magnetic hysteresis on HF injection based inductance calculation'. Proc. of Energy Conversion Congress and Exposition (ECCE 2011), Phoenix, AZ, USA, September 17–22 2011, pp. 638–645

## 8 Appendix

**Table 1** 11 kW SynRM parameters

| Parameter symbol | Parameter value |
|---|---|
| $R_s$ | 0.72 Ω |
| $L_{sda}$ (linear region) | 80 mH |
| $L_{sqa}$ (linear region) | 60 mH |
| $p$ | 2 |
| $u_n$ | 400 V |
| $i_n$ | 18 A |
| $\omega_n$ | 647.05 rad/s |
| $\tau_n$ | 17 N m |
| $J_m$ (SynRM) | 0.00351 kg m$^2$ |
| $J_m$ (complete back-to-back connection) | 0.034 kg m$^2$ |
| $B_m$ | $10{\cdot}10^{-3}$ N ms/rad |